

## Tuning molecule-substrate coupling *via* deposition of metal adatoms

Hung-Hsiang Yang,<sup>1</sup> Hsu-Han Tsai,<sup>2</sup> Chi-Feng Ying,<sup>2</sup> Tsung-Han Yang,<sup>3</sup>  
 Chao-Cheng Kaun,<sup>3,a)</sup> Chun-hsien Chen,<sup>2,4,b)</sup> and Minn-Tsong Lin<sup>1,5,c)</sup>

<sup>1</sup>Department of Physics, National Taiwan University, Taipei 10617, Taiwan

<sup>2</sup>Department of Chemistry, National Taiwan University, Taipei 10617, Taiwan

<sup>3</sup>Research Center for Applied Sciences, Academia Sinica, Taipei 11529, Taiwan

<sup>4</sup>Center for Emerging Material and Advanced Device, National Taiwan University, Taipei 10617, Taiwan

<sup>5</sup>Institute of Atomic and Molecular Sciences, Academia Sinica, Taipei 10617, Taiwan

(Received 17 June 2015; accepted 3 November 2015; published online 12 November 2015)

Organic-inorganic hybrids constitute an important class of functional materials. The fundamentals at the molecular levels are, however, relatively unexplored. PTCDA (perylene-3,4,9,10-tetracarboxylic dianhydride) is a colorant and extensively applied in organic-based optoelectronic devices. PTCDA/Cu(111) and Fe-PTCDA/Cu(111) metal-organic hybrid monolayers are studied by low temperature scanning tunneling microscopy and spectroscopy (STS) and density functional theory (DFT). The former exhibits Moiré pattern-modulated molecular density of states while the latter adapts a commensurate adlattice. Both imaging and spectroscopic results suggest a strong hybridization between PTCDA molecules and Cu(111) substrate. Weak PTCDA-Cu(111) coupling can be obtained by the introduction of Fe adatoms. Compared to PTCDA/Cu(111), STS spectra of Fe-PTCDA/Cu(111) exhibit a higher energy and sharper features of the frontier orbitals. Together with the DFT results, we found that the PTCDA-Cu(111) coupling is attenuated by the presence of Fe adatoms and Fe-PTCDA coordination. © 2015 AIP Publishing LLC. [<http://dx.doi.org/10.1063/1.4935714>]

### INTRODUCTION

Molecule-substrate coupling strongly influences electron-transporting properties of organic devices, such as organic light-emitting diodes, field-effect transistors, organic solar cells, and organic spin valves.<sup>1–5</sup> Electron transport through metal-organic heterojunctions in organic electronics mostly depends on the interface formed between the metal atom and the organic molecule in terms of geometric and electronic configurations.<sup>6</sup> To tailor the properties of organic devices, it requires not only detailed understanding of mechanisms at the metal-organic interface but also the ability to adjust the coupling between organic adsorbate and metal substrate. Introducing a dielectric layer in between organic/metal substrate is a recent approach to modify the electronic interactions.<sup>7–9</sup> Such a layer successfully weakens the hybridization between molecules and the metal substrate but results in strong nonlinearities of the charge transport in organic electronics. Another approach, demonstrated by Franke *et al.*,<sup>10</sup> to reduce the molecule-substrate coupling is having molecules lifted away from the substrate by introducing a different species of molecule. In their case of 1,3,5,7-tetraphenyladamantane (TPA)/C<sub>60</sub> tetramer, the C<sub>60</sub>-substrate spacing was hoisted by TPA and therefore reducing the hybridization between C<sub>60</sub> and the substrate. This approach utilizes bulky molecules which inherit weak intermolecular interactions. However, it appears less appropriate for

those preferable to optoelectronic applications because the molecules often adopt high planarity and functional groups that aggregation and molecule-substrate anchoring hamper the insertion of the abovementioned bulky molecule.

Here we propose an alternative to adjust the degree of molecule-substrate hybridization through introducing additional interactions to the molecule. The rationale is simple: the additional interactions weaken the molecule-substrate coupling. What we will demonstrate is metal-organic coordination *via* which 2D lattices have been patterned.<sup>11,12</sup> Accompanying changes are the oxidation states and the strength of metal-organic interactions involved in the coordination reaction.<sup>13–15</sup> Hence, the model compound is planar PTCDA (perylene-3,4,9,10-tetracarboxylic dianhydride). The assembly of PTCDA on Cu(111) exhibits significant strong molecule-substrate hybridization which strongly correlates to the degree of charge transfer.<sup>16–20</sup> To change the molecular bonding environments, Fe atoms are introduced to coordinate PTCDA (see Method). We will show that the degree of PTCDA-Cu(111) hybridization becomes smaller than that without Fe adatoms.

### RESULTS AND DISCUSSION

Figure 1(a) shows a typical STM image of submonolayer PTCDA on Cu(111). The molecules adapt close-packed herringbone arrangement which suggests the presence of significant intermolecular attractions. Figure 1(a) exhibits characteristics of a superlattice with some PTCDA brighter than their neighboring ones. Figure 1(b) displays the

a)Electronic mail: kaunc@gate.sinica.edu.tw

b)Electronic mail: chhchen@ntu.edu.tw

c)Electronic mail: mtlin@phys.ntu.edu.tw

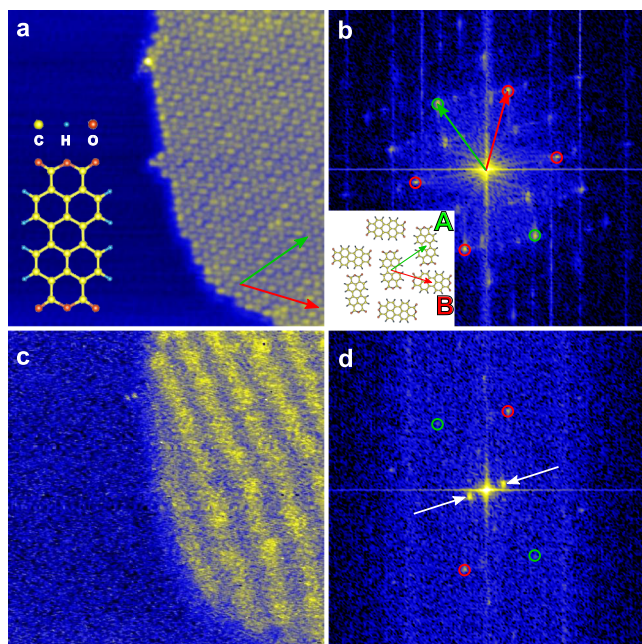


FIG. 1. PTCDA submonolayer on Cu(111): (a) STM image, (b) FFT image, (c)  $dI/dV$  map acquired simultaneously with panel (a), and (d) FFT image of panel (c). Unit cell vectors in panel (b), green and red arrows, correspond, respectively, to molecule sites A and B (see text). To facilitate the identification of the corresponding directions in real space, the arrows are illustrated in panel (a) with an enlarged magnitude (*ca.* 10 times longer). White arrows indicate the periodicity of the Moiré pattern. Inset: (a) chemical structure of PTCDA; (b) a proposed real-space model. The modulation voltage,  $\Delta U$ , for STS measurements was 30 mV. Other conditions:  $E_{bias}$ , 0.4 V; size, ((a) and (c))  $40 \times 40 \text{ nm}^2$ , (b) and (d))  $4 \times 4 \text{ nm}^{-2}$ .

corresponding FFT (Fast Fourier Transform) image with hexagonal reciprocal lattice points. The unit vectors are indicated by green and red arrows and yield a unit cell dimension of 0.94 nm. Almost all spots in the FFT image can be reproduced by considering the periodicities from one and multiple-integer times unit cells.<sup>21</sup> Based on the FFT image and the real space images, proposed in the inset is a plausible PTCDA/Cu(111) model, in a good agreement with the literature reports by Wagner and co-workers.<sup>22,23</sup> The molecules have two orientations with the long molecular axes nearly vertical to each other. The corresponding unit vectors are superimposed onto the real-space model. We state A (B) for molecules indicated by green (red) arrows in the following discussions. As concluded by Wagner *et al.*,<sup>22</sup> the unit vectors of the PTCDA self-assembled layer is described by the matrix,  $\begin{pmatrix} a \\ b \end{pmatrix} = \begin{pmatrix} 1 & 5 \\ 9 & 3 \end{pmatrix} \begin{pmatrix} a_{Cu} \\ b_{Cu} \end{pmatrix}$ , where  $a_{Cu}$  and  $b_{Cu}$  are the unit vectors of the Cu(111) surface. The non-integer coefficients indicate an incommensurate growth of PTCDA/Cu(111).

Figure 1(c) shows a conductance map (acquired by using lock-in techniques) taken simultaneously with Figure 1(a). The electronic contrast reveals striped corrugations. The FFT image (Figure 1(d)) shows two spots, corresponding to the period of the ordered stripes (marked by white arrows). The periodicity of the unit cell remains visible while signals from molecule A and B vary in intensity. This indicates that A and B are electronically inequivalent. The variation on the electronic structure is consistent with incommensurate adlattice which bears different contact configurations and thus molecule-

substrate coupling. Accordingly, the incommensuration indicates mismatch between the dimensions of PTCDA herringbone structure and Cu(111) lattice.<sup>22</sup> The corrugations in the conductance map are henceforth assigned to a Moiré pattern.

The Moiré pattern is further examined by high resolution images (*e.g.*, Figure 2(a)). Detailed features suggest that molecule A (B) is in fact composed of A1 (B1) and A2 (B2). To explain the modulation in the images, scanning tunneling microscopy and spectroscopy (STS) is carried out. The spectra (Figure 2(b)) are not identical, manifesting that the discrepancy in images is arising from their electronic structures. The inset of Figure 2(b) presents a molecular orbital resolved STM image (at  $E_{bias} = -0.5 \text{ V}$ ) with two lobes in the outer and three in the inner part. Displayed next to the image is the corresponding simulation result. The distribution of charge density, which coincides with the image, portrays the LUMO (lowest unoccupied molecular orbital) of PTCDA by DFT (density functional theory) calculations for a gas-phase molecule.<sup>15</sup> The image and the simulation shows mirror symmetry along both the short and long molecular axes.

The characteristics of LUMO are observed at a negative  $E_{bias}$ . The STS spectra of PTCDA show a broad peak concurred with the surface state of Cu(111). Hence, charge transfer from Cu(111) to PTCDA develops an occupied LUMO and yields a strong adsorbate-substrate hybridization.<sup>16,24,25</sup>

The ability to adjust the interactions at the organic/inorganic interface plays an essential role to engineer the properties of organic devices. To modify the degree of the electronic coupling between PTCDA and the substrate, Fe adatoms are introduced. Figure 3 shows the co-deposited Fe-PTCDA/Cu(111) assembly, analogous to the ladder-like structure of Fe-PTCDA grown on Au(111).<sup>15,26</sup> Based on the positions in the ladder, chain- and rung-PTCDA are denoted for the molecules (Figure 4(a)). Fe-PTCDA islands have preferred directions (arrows in Figure 3(a)) on the Cu(111) lattice (inset). The chain molecules tend to grow along the directions with an angle difference  $\sim 30^\circ$  respecting to Cu(111) unit vectors. This finding is confirmed by the FFT image (*e.g.*, Figure 3(b)) in which the hexagonal pattern bears three-fold symmetry and rotates an angle of  $\sim 30^\circ$  from that of the Cu(111) substrate (inset). No indication of Moiré pattern can be found from STM images and  $dI/dV$  conductance maps.<sup>21</sup>

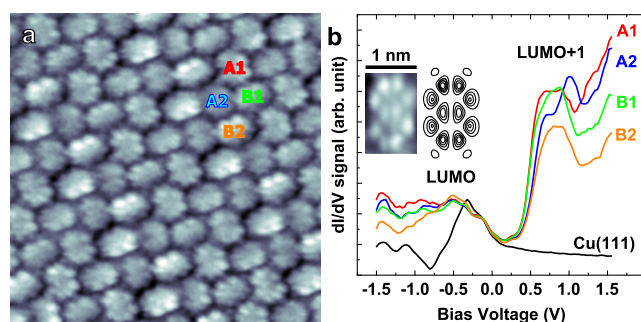


FIG. 2. (a) STM image and (b) STS spectra of PTCDA on Cu(111). The traces are color-coded to represent spectra over PTCDA with different bonding environments. Inset: STM image ( $E_{bias} = -0.5 \text{ V}$ ) of one PTCDA molecule and the corresponding charge density of LUMO by DFT simulations.<sup>15</sup> Other conditions:  $E_{bias}$ ,  $-0.5 \text{ V}$ ;  $\Delta U$ , 30 mV; size,  $10 \times 10 \text{ nm}^2$ .

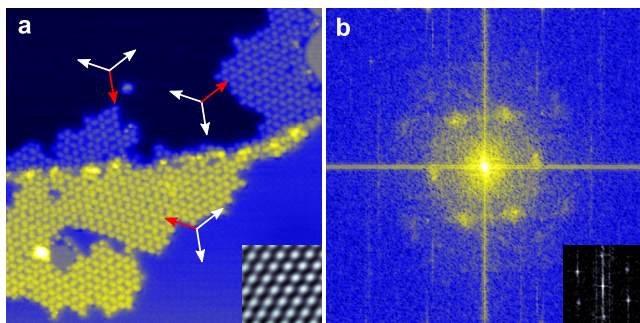


FIG. 3. (a) STM image and (b) the corresponding FFT image of Fe-PTCDA on Cu(111). Arrows illustrate the three-fold symmetry of PTCDA at the chain sites. ( $50 \times 50 \text{ nm}^2$ ,  $E_{\text{bias}} = 0.5 \text{ V}$ ) Inset: (a) image ( $1.5 \times 1.5 \text{ nm}^2$ ,  $E_{\text{bias}} = 30 \text{ mV}$ ) and (b) FFT image of the underneath Cu(111).

It is peculiar that the topographic images and  $dI/dV$  maps do not disclose the deposited Fe adatoms. Similar perplexities were encountered in our previous Fe-PTCDA/Au(111) study<sup>15</sup> in which DFT simulations suggest Fe atoms being coordinated to and positioned under curved and elevated PTCDA. Considering the analogy for the two cases, the binding scheme is scrutinized for the present study of Fe-PTCDA/Cu(111).

Figure 4(a) (Figure 4(b)) shows, at bias voltage of  $0.5 \text{ V}$  ( $-0.5 \text{ V}$ ), a high resolution STM image of the Fe-PTCDA network with Fe-PTCDA chains interconnected by rung PTCDA molecules.<sup>15</sup> At the molecular termini, additional protrusions are observed at both  $0.5$  and  $-0.5 \text{ V}$  (marked by green circles). Such protrusions are usually assigned to the locations of the coordinated metal atoms,<sup>27–30</sup> in this case,

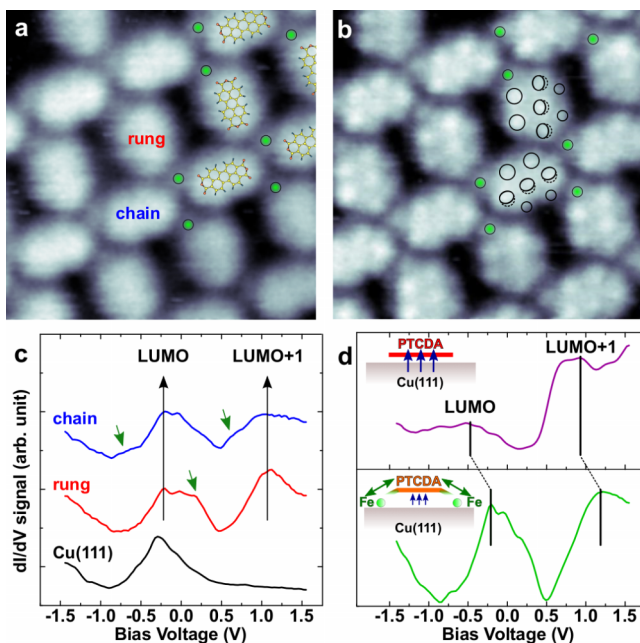


FIG. 4. ((a) and (b)) STM images and (c) STS spectra of Fe-PTCDA on Cu(111). (d) Comparison of the STS spectra between PTCDA/Cu(111) (upper panel) and Fe-PTCDA/Cu(111) (lower panel). Imaging features were  $E_{\text{bias}}$ -dependent ((a)  $0.5 \text{ V}$ ; (b)  $-0.5 \text{ V}$ ). STS spectra were acquired on rung- (red) and chain-PTCDA (blue) and that averaged over several unit cells (green). Spectra of bare Cu(111) (black) and PTCDA/Cu(111) (purple) are also provided for comparison. Illustrations are plausible models. Green circles present Fe atoms. Other conditions:  $\Delta U$ ,  $30 \text{ mV}$ ; size,  $5 \times 5 \text{ nm}^2$ .

the Fe atoms. According to previous studies,<sup>15,26</sup> a tentative model of the Fe-PTCDA network on Cu(111) is proposed and superposed onto the STM image (upper right corner of Figure 4(a)). Thereby, chain- and rung-PTCDA coordinate with four and two Fe atoms, respectively. Figure 4(b) shows the intramolecular resolution of the Fe-PTCDA structure at  $-0.5 \text{ V}$ . The intramolecular structure has the characteristics of LUMO but less symmetric than those of PTCDA/Cu(111). The outer lobes show different sizes and the inner lobes tend to overlap between sets of lobes (black portrays). The deformed LUMO feature is consistent with tilted molecules after coordinating with Fe atoms.<sup>21</sup>

Figures 4(c) and 4(d) summarize STS results of Fe-PTCDA/Cu(111). The red (blue) curve is taken at the center of rung-PTCDA (chain-PTCDA). Pronounced peaks are found at bias voltage at around  $-0.2 \text{ V}$  and  $1.2 \text{ V}$  on both rung- and chain-PTCDA. The black curve shows the typical feature of the Shockley surface state on Cu(111). Taking together the STS and STM results, we conclude that the peak at  $-0.2 \text{ V}$  arises from the LUMO of PTCDA. In addition, green arrows mark the difference between the spectra. Considering the distinct binding environments of rung- and chain-PTCDA, their spectral disparities are ascribed to different number of Fe atoms connecting to the PTCDA molecules. Hence these features pinpointed by the arrows demonstrate the presence of Fe-PTCDA interactions.

Figure 4(d) presents averaged STS results of PTCDA/Cu(111) (upper panel) and Fe-PTCDA/Cu(111) (lower panel). They are different in peak positions and broadness. The black vertical lines indicate the energy levels of frontier molecular orbitals (FMOs). The incorporation of Fe adatoms into the PTCDA monolayer shifts the energy levels *ca.*  $300 \text{ mV}$  more positively, suggesting less significant electron transfer to the FMOs of PTCDA from Cu(111). The weakened electronic coupling between Fe-PTCDA and Cu(111) is also confirmed by the relative sharpness of the FMO peaks,<sup>21</sup> given that strong molecule-substrate interaction generally yields broadened bands for FMOs. Illustrations in Figure 4(d) propose plausible models. The introduction of Fe atoms diminishes the interactions between molecules and Cu(111) (presented by dark blue arrows, the bigger the arrow size the larger hybridization) and additional hybridized Fe-PTCDA states are developed (green arrows).

To further address how the co-adsorbed Fe diminishes the PTCDA-Cu(111) interactions, DFT calculations are carried out (Figure 5). The optimized structure of the PTCDA/Cu(111) is presented in Figure 5(a), including views along unit vector  $\vec{c}$  (left panel) and  $\vec{a}$  (right panel). The PTCDA-Cu(111) distance is found around  $2.77 \text{ \AA}$ , in good agreement with the literatures<sup>17,19</sup> in which a strong PTCDA-Cu(111) interaction is concluded. Figure 5(b) shows the DOS of the self-assembled PTCDA layer (solid curve) and the underlying Cu(111) surface (dashed curve). The LUMO is found occupied, consistent with the STS results (Figure 2(b)). Near the Fermi level, the main features of the DOS of the PTCDA molecules coincide with the underlying Cu(111) surface, indicating a strong PTCDA-Cu(111) hybridization.

To achieve the structure relaxation of Fe-PTCDA/Cu(111), a more symmetrical structure is constructed<sup>31</sup> and

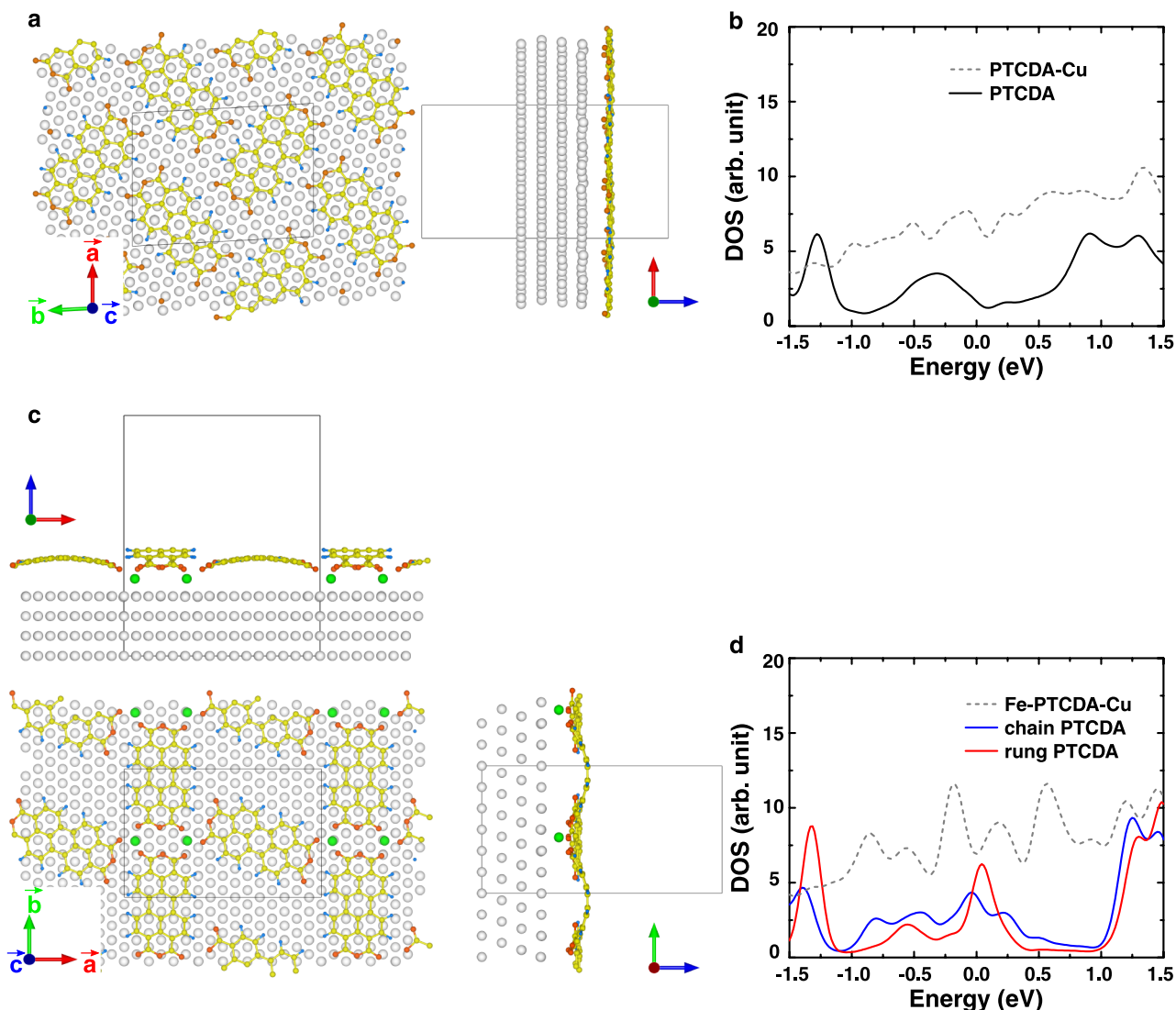


FIG. 5. (a) Optimized structure of PTCDA/Cu(111). Left panel: the view along unit vector  $\vec{c}$ . Right panel: the view along unit vector  $\vec{a}$ . (b) DOS of the PTCDA molecule in the herringbone structure (named PTCDA, solid curve) and the underneath Cu surface (named PTCDA-Cu, dashed curve). (c) Optimized structure of Fe-PTCDA/Cu(111). Upper panel: the view along unit vector  $\vec{a}$ . Right panel: the view along unit vector  $\vec{b}$ . Middle panel: the view along unit vector  $\vec{c}$ . (d) DOS of the chain (blue) and rung (red) PTCDA molecules in the Fe-PTCDA/Cu(111) hybrid and the underneath Cu surface (named Fe-PTCDA-Cu, dashed curve).

presented in Figure 5(c) with views along three unit vectors (upper panel:  $\vec{a}$ , right panel:  $\vec{b}$ , and middle panel:  $\vec{c}$ ). After incorporating with Fe atoms, PTCDA molecules are bent and lifted away from the Cu(111) surface. The central carbon atom of the chain (rung) PTCDA resides  $\sim 4.79$  Å ( $\sim 3.98$  Å) above the substrate, significantly longer than that of 2.77 Å (Figure 5(a)). Accordingly, a weaker PTCDA-Cu(111) interaction is expected. The calculated DOS of the Fe-PTCDA structure is displayed in Figure 5(d). Instead of an occupied and broadened LUMO in PTCDA/Cu(111) (Figure 5(a)), both chain and rung molecules exhibit partially occupied LUMO and sharper features of the DOS. In the energy range  $[-0.25, 0.25]$  eV, the DOS of both chain and rung molecules deviate from the main features of the underneath substrate (dashed, termed Fe-PTCDA-Cu in Figure 5(d)), indicating a relatively weak PTCDA-Cu(111) hybridization. Furthermore, the differences of the DOS between chain and rung molecules generally agrees with the STS measurements. Considering

the larger molecule-substrate distance, the sharper and up-shifted molecular orbitals, we found that the PTCDA-Cu(111) interactions are weakened after the formation of the Fe-PTCDA hybrid.

## CONCLUSION

In conclusion, we have grown self-assembled PTCDA monolayer and the well-ordered Fe-PTCDA complex on the Cu(111) surface. Strong hybridization between PTCDA molecules and the Cu(111) substrate is identified. DFT results evidence that the PTCDA molecules are lifted after coordinating with Fe atoms. Consequently, the coupling between PTCDA molecules and Cu(111) is reduced in this matter. Our finding shows that by forming the metal-organic complex, the molecule-substrate coupling can be tuned, representing an alternative to engineer the metal-organic interfaces.

## METHOD

Measurements were performed in a ultra-high vacuum scanning tunneling microscope (Unisoku, USM-1400) at 78 K using electrochemically etched tungsten tips. Cu(111) surface (MaTeck) was cleaned by cycles of Ar<sup>+</sup> sputtering ( $5 \times 10^{-5}$  mbar; 1 kV) and annealing (~900 K). For scanning tunneling spectroscopy, a modulation voltage ( $\Delta U = 30$  mV,  $f = 3$  kHz) is added to the bias voltage and the induced current modulation recorded *via* lock-in techniques. All images were taken by constant current mode. The reported  $E_{bias}$  was the voltage with bias voltages applied on the sample against that of the tip. PTCDA/Cu(111) was prepared by depositing PTCDA (Aldrich) onto substrate at room temperature. For Fe-PTCDA/Cu(111), PTCDA and Fe (Alfa Aesar) were co-deposited onto room-temperature sample surface (with the coverage ratio between Fe and PTCDA around 1:3).<sup>21</sup> After a final annealing step to ~400 K, Fe-PTCDA networks were formed. All images are processed by Nanotech WSxM.<sup>32</sup>

All geometry structures were optimized with VASP package,<sup>33</sup> with the paw-GGA pseudopotential. Since the van der Waals force is important to the PTCDA adsorption on copper surface, the vdW-DFT functional was adopted.<sup>34,35</sup> For structural relaxation, the kinetic energy cutoff of plane wave basis was 300 eV at  $\Gamma$ , as the atomic force was smaller than 0.02 eV/Å. The first layer of Cu(111) was allowed to move during the geometry optimization. Both herringbone PTCDA and Fe-PTCDA were placed on four layers of Cu(111). The supercell size and PTCDA ordering of herringbone PTCDA on Cu(111) have been studied.<sup>20,22</sup> For electronic properties, the kinetic energy cutoff of plane wave basis was 400 eV. The  $4 \times 3 \times 1$  and  $3 \times 4 \times 1$  k-points were adopted to sample the Brillouin zone of herringbone PTCDA and Fe-PTCDA on Cu(111), respectively. The converged criterion was  $10^{-4}$  eV.

## ACKNOWLEDGMENTS

Financial support by the Ministry of Science and Technology (MOST). The authors are grateful for stimulating discussions with Yu-Hsun Chu.

<sup>1</sup>E. Moons, *J. Phys.: Condens. Matter* **14**, 12235 (2002).

<sup>2</sup>F. Cicoira and C. Santato, *Adv. Funct. Mater.* **17**, 3421 (2007).

<sup>3</sup>P. W. M. Blom, V. D. Mihailetschi, L. J. A. Koster, and D. E. Markov, *Adv. Mater.* **19**, 1551 (2007).

<sup>4</sup>C. J. Brabec, N. S. Sariciftci, and J. C. Hummelen, *Adv. Funct. Mater.* **11**, 15 (2001).

<sup>5</sup>C. Barraud, P. Seneor, R. Mattana, S. Fusil, K. Bouzehouane, C. Deranlot, P. Graziosi, L. Hueso, I. Bergenti, V. Dediu, F. Petroff, and A. Fert, *Nat. Phys.* **6**, 615 (2010).

<sup>6</sup>G. V. Nazin, X. H. Qiu, and W. Ho, *Science* **302**, 77 (2003).

<sup>7</sup>I. Swart, T. Sonleitner, and J. Repp, *Nano Lett.* **11**, 1580 (2011).

<sup>8</sup>L. Gross, N. Moll, F. Mohn, A. Curioni, G. Meyer, F. Hanke, and M. Persson, *Phys. Rev. Lett.* **107**, 086101 (2011).

<sup>9</sup>F. Mohn, L. Gross, N. Moll, and G. Meyer, *Nat. Nanotechnol.* **7**, 227 (2012).

<sup>10</sup>K. Franke, G. Schulze, N. Henningsen, I. Fernández-Torrente, J. Pascual, S. Zarwell, K. Rück-Braun, M. Cobian, and N. Lorente, *Phys. Rev. Lett.* **100**, 036807 (2008).

<sup>11</sup>S. Stepanow, N. Lin, D. Payer, U. Schlickum, F. Klappenberger, G. Zoppellaro, M. Ruben, H. Brune, J. V. Barth, and K. Kern, *Angew. Chem., Int. Ed.* **46**, 710 (2007).

<sup>12</sup>S. Klyatskaya, F. Klappenberger, U. Schlickum, D. Kühne, M. Marschall, J. Reichert, R. Decker, W. Krenner, G. Zoppellaro, H. Brune, J. V. Barth, and M. Ruben, *Adv. Funct. Mater.* **21**, 1230 (2011).

<sup>13</sup>U. Schlickum, F. Klappenberger, R. Decker, G. Zoppellaro, S. Klyatskaya, M. Ruben, K. Kern, H. Brune, and J. V. Barth, *J. Phys. Chem. C* **114**, 15602 (2010).

<sup>14</sup>Y. Li, J. Xiao, T. E. Shubina, M. Chen, Z. Shi, M. Schmid, H.-P. Steinrück, J. M. Gottfried, and N. Lin, *J. Am. Chem. Soc.* **134**, 6401 (2012).

<sup>15</sup>H.-H. Yang, Y.-H. Chu, C.-I. Lu, T.-H. Yang, K.-J. Yang, C.-C. Kaun, G. Hoffmann, and M.-T. Lin, *ACS Nano* **7**, 2814 (2013).

<sup>16</sup>F. Tautz, *Prog. Surf. Sci.* **82**, 479 (2007).

<sup>17</sup>A. Gerlach, S. Sellner, F. Schreiber, N. Koch, and J. Zegenhagen, *Phys. Rev. B* **75**, 045401 (2007).

<sup>18</sup>S. Henze, O. Bauer, T.-L. Lee, M. Sokolowski, and F. Tautz, *Surf. Sci.* **601**, 1566 (2007).

<sup>19</sup>S. Duhm, A. Gerlach, I. Salzmann, B. Bröker, R. Johnson, F. Schreiber, and N. Koch, *Org. Electron.* **9**, 111 (2008).

<sup>20</sup>L. Romaner, D. Nabok, P. Puschnig, E. Zojer, and C. Ambrosch-Draxl, *New J. Phys.* **11**, 053010 (2009).

<sup>21</sup>See supplementary material at <http://dx.doi.org/10.1063/1.4935714> for multiple unit cell grid on the FFT image, absence of Moiré pattern in the conductance map of Fe-PTCDA, Gaussian fitting of the FMO peaks, projections of simulated LUMO with various tilted angles and STM images of different Fe and PTCDA coverage ratios.

<sup>22</sup>T. Wagner, A. Bannani, C. Bobisch, H. Karacuban, and R. Möller, *J. Phys.: Condens. Matter* **19**, 056009 (2007).

<sup>23</sup>M. C. Cottin, J. Schaffert, A. Sonntag, H. Karacuban, R. Möller, and C. A. Bobisch, *Appl. Surf. Sci.* **258**, 2196 (2012).

<sup>24</sup>R. Temirov, S. Soubatch, A. Luican, and F. S. Tautz, *Nature* **444**, 350 (2006).

<sup>25</sup>J. K. Norsko, *Rep. Prog. Phys.* **53**, 1253 (1990).

<sup>26</sup>L. Alvarez, S. Peláez, R. Caillard, P. A. Serena, J. A. Martín-Gago, and J. Méndez, *Nanotechnology* **21**, 305703 (2010).

<sup>27</sup>T.-C. Tseng, N. Abdurakhmanova, S. Stepanow, and K. Kern, *J. Phys. Chem. C* **115**, 10211 (2011).

<sup>28</sup>M. Piantek, D. Serrate, M. Moro-Lagares, P. Algarabel, J. I. Pascual, and M. R. Ibarra, *J. Phys. Chem. C* **118**, 17895 (2014).

<sup>29</sup>C. S. Kley, J. Čechal, T. Kumagai, F. Schramm, M. Ruben, S. Stepanow, and K. Kern, *J. Am. Chem. Soc.* **134**, 6072 (2012).

<sup>30</sup>J. Čechal, C. S. Kley, T. Kumagai, F. Schramm, M. Ruben, S. Stepanow, and K. Kern, *J. Phys. Chem. C* **117**, 8871 (2013).

<sup>31</sup>Comparing to the structure in Figure 4a, a more symmetrical structure is chosen to reduce the calculation costs. Nevertheless, the essential physics on the Fe incorporation are carried out by the calculated DOS results.

<sup>32</sup>I. Horcas, R. Fernández, J. M. Gómez-Rodríguez, J. Colchero, J. Gómez-Herrero, and A. M. Baro, *Rev. Sci. Instrum.* **78**, 013705 (2007).

<sup>33</sup>G. Kresse and J. Furthmüller, *Phys. Rev. B* **54**, 11169 (1996).

<sup>34</sup>J. Klimeček, D. R. Bowler, and A. Michaelides, *J. Phys.: Condens. Matter* **22**, 022201 (2010).

<sup>35</sup>J. C. V. Klimeš, D. R. Bowler, and A. Michaelides, *Phys. Rev. B* **83**, 195131 (2011).